The solvent effect on the electrocatalytic cleavage of carbon-halogen bonds on Ag and Au

Serena Arnaboldi[a]*, Armando Gennaro[b], Abdirisak Ahmed Isse[b]*, Patrizia Romana Mussini[a]

[a]*Department of Chemistry, University of Milan, Via Golgi 19, 20133 Milano, Italy;*

email addresses: serena.arnaboldi@unimi.it, patrizia.mussini@unimi.it.

[b]*Department of Chemical Sciences, University of Padova, via Marzolo 1, 35131 Padova, Italy;*

email addresses: armando.gennaro@unipd.it, abdirisak.ahmedisse@unipd.it.

Corresponding authors:

A.A. Isse, *abdirisak.ahmedisse@unipd.it*.

S. Arnaboldi, *serena.arnaboldi@unimi.it*.

Abstract

In recent years it has been shown in detail how the electrocatalytic cleavage of carbon-halogen bonds is modulated by (a) the stepwise or concerted nature of the dissociative electron-transfer mechanism, which is influenced by the nature of the electrode surface, the type of halogen atom and the molecular structure of RX as a whole, and (b) the double-layer structure (as a function of the nature and bulkiness of the supporting electrolyte ions). In order to both complete and support the interpretative scheme thus developed, this work is focused on the solvent role. When one compares aprotic with protic organic solvents after appropriate intersolvental normalization, interesting peculiarities emerge, especially concerning protic media. Solvent proticity deeply affects both the reaction mechanism (on both non-catalytic and catalytic electrodes) and the extent of the catalytic effects. These items are discussed on the basis of a complete investigation carried out with a carefully controlled experimental protocol on two chloride and bromide couples, one aromatic and one aliphatic, representative of stepwise and concerted mechanisms, respectively, in four aprotic and four protic solvents, on both non–catalytic GC and catalytic Ag and Au electrodes. The results are discussed in the framework of a recently developed interpretative scheme of the carbon-halogen cleavage mechanism.

Keywords: Dissociative electron transfer, electrocatalysis, solvent effect, reductive cleavage, carbon-halogen bond

1. Introduction

The electroreductive cleavage of carbon–halogen bonds is a fundamental process in molecular electrochemistry, with many applications in the synthetic, analytical and environmental fields [1]. It also provides an excellent model for mechanistic studies on dissociative electron transfer (DET) [2].

The electroreductive cleavage of organic halides (RXs) proceeds *via* a DET to yield a radical $R^{\bullet}$ and an anion X^{-}, often followed by reduction of the radical to the corresponding carbanion R^{-}. The mechanism of DET to RX on non-catalytic electrodes, such as glassy carbon (GC), is well understood. It can occur along two mechanisms, concerted and stepwise. In the first one, typical of aliphatic halides, electron transfer (ET) and bond breaking are concurrent and directly result in the formation of $R^{\bullet}$ and X^{-}:

$$RX + e^{-} \rightarrow R^{\bullet} + X^{-} \qquad (1)$$

In the stepwise mechanism, typical of aryl halides, a first rather fast ET results in the formation of a radical anion $RX^{\bullet -}$, which subsequently undergoes cleavage of the C–X bond to give $R^{\bullet}$ and X^{-}:

$$RX + e^{-} \leftrightarrows RX^{\bullet -} \qquad (2)$$

$$RX^{\bullet -} \rightarrow R^{\bullet} + X^{-} \qquad (3)$$

Accordingly, two activation barriers related to the ET and cleavage steps must be considered in the stepwise case. The relative heights of these barriers can be accounted for by a diagnostic parameter κ obtainable in voltammetric experiments [3].

In recent decades, research has been concentrated on the use of catalytic metal surfaces, able to interact with RX and its reduction intermediates and products, thus modifying the whole reaction pathway. Such electrocatalytic conditions allow working at remarkably milder potentials, and in many cases improve the selectivity of the reaction and/or significantly affect the nature of the reduction products. Pd [4-11], Cu [10-12] and, above all, Ag [3,13-19] have high and reproducible catalytic activities for the electrochemical reduction of organic halides, whereas milder and/or less reproducible activities are exhibited by other metals including Hg, Pb and Au [13,14]. Actually, according to theoretical studies, Au has the highest intrinsic affinity for halide anions [20,21], which is confirmed by experimental determination of the amount of halide anions specifically adsorbed on different metals in water at the potential of zero charge (PZC), showing the following order of increasing affinity [22,23]:

$$\text{Bi, Pb} < \text{Hg} < \text{Cd, Ga} < \text{Cu (111)} < \text{Ag(111)} < \text{Au(111)}$$

Accordingly, Au is expected to possess higher catalytic properties than metals such as Ag and Cu. However, the PZC of Au (–0.05 V *vs* SCE in $NaClO_4$ aqueous solution [24]) is so high that in the potential range typical of RX reduction, the Au surface bears a large negative charge, which considerably decreases the affinity of the metal for X^-, resulting in a significantly reduced catalytic activity. Conversely, the PZC of Ag is quite negative (–0.96 V *vs* SCE [25]) and in the potential range typical of RX reduction the metal essentially preserves its affinity for X^-. Consequently, Ag exhibits better catalytic activities than Au for RX reduction.

Detailed mechanistic analyses of the electrocatalytic process have been so far achieved for the reduction of aryl [3] and benzyl halides [16,17], in the latter case also with the support of a combined computational and SERS investigation [26,27], even if the computation-based mechanism published in reference [27] has recently been disproved by the same authors [28], agreeing with a previously published mechanism [16]. In the same context, detailed studies have been carried out on the role of single factors modulating the process, such as the reactant molecular structure (organic moiety and halide leaving group), the nature, morphology and state of the electrode surface [29], the adsorption of the reagents and products [30,31], and the role of the supporting electrolyte [32], while few preliminary studies have been reported concerning the role of the solvent [33-35], and a more systematic investigation is still overdue.

Solvation is a key factor in ET processes (as implied *inter alia* by the importance of the solvent reorganization energy λ_o in Marcus theory of ET [2]) as it modifies the free energy profile along the reaction coordinate. This modulation can be huge and is typically asymmetric for DET processes, since a polar solvent, like acetonitrile, will preferentially stabilize the species having the highest charge density, such as the halide anions resulting from the process; thus solvation affects both the process thermodynamics and kinetics [35]. At the same time the solvent also affects the rate of mass transfer (through its viscosity) and the extent and mode of specific adsorption processes.

Several studies on the solvent effect on RX reduction are available for specific cases in non-catalytic conditions. For instance, Savéant and co-workers [36] studied the stability of ion-radical adducts in different solvents, demonstrating that the interaction energy between $R^\bullet$ and X^- is inversely proportional to the solvent polarity and its solvation capability, whereas Fedurco *et al.* [37], working on a class of methyl and methylene halides, observed a dramatic increase in the ET kinetics in aqueous solution in comparison with the same process in N,N'–dimethylformamide.

More recently, a preliminary study of the solvent effect under catalytic *vs* non-catalytic conditions (Ag *vs* GC) was carried out [33] by investigating DET to two organic bromides (acetobromoglucose and benzyl bromide) in five aprotic solvents (acetone, dimethylformamide, acetonitrile, propylene carbonate, dimethyl sulfoxide) and only one protic solvent, namely, methanol. The study confirmed the key roles of both the halide anion solvation capability (in terms of primary medium effect) and solvent proticity, with methanol affording the least negative reduction potentials both on non–catalytic and catalytic electrodes, and the highest catalytic effects.

However, a more complete and systematic study is overdue, especially considering the following points: (i) extending the protic series to modulate parameters such as pK_a, relative permittivity, and ability of the solvent to specifically adsorb onto the catalytic surface; (ii) using RX model compounds that are representative of both DET mechanisms and the X^- leaving group; (iii) including Au as a catalytic material and looking for favourable solvent conditions in which its high intrinsic affinity for X^- can be better exploited. The work reported herein was designed along these lines. Accordingly, an exhaustive voltammetric investigation on the set of model molecules depicted in Fig. 1 was carried out along a strict protocol in four aprotic solvents (acetone, dimethylformamide, acetonitrile and dimethyl sulfoxide) and four protic solvents (n-butanol, n-propanol, ethanol and methanol). Some physical and chemical properties of the solvents are summarized in Table 1. As shown, the selected set of solvents covers a wide range of viscosity, relative permittivity and, in the case of the alcohols, autoprotolysis constant. The study also compares three different electrodes: Au, Ag and glassy carbon (GC), the latter taken approximately as a non-catalytic surface towards reductive cleavage of carbon-halogen bonds [38].

2. Experimental

Acetonitrile (MeCN), dimethyl sulfoxide (DMSO), dimethylformamide (DMF), acetone (AC), methanol (MeOH), ethanol (EtOH), n-propanol (n-PrOH) and n-butanol (n-BuOH) were purchased from Aldrich (HPLC grade or equivalent). Organic halides (Fig. 1) were obtained from Aldrich or Fluka (analytical grade). Tetra-n-butylammonium tetrafluoroborate (n-Bu_4NBF_4), used as background electrolyte at a concentration of 0.1 M, was obtained from Fluka (reagent grade). All chemicals were used as received.

Cyclic voltammetry was carried out on deaerated solutions (4 cm^3) in a three-electrode mini-cell thermostated at 298 K, with an Autolab PGSTAT 12 or 30 potentiostat/galvanostat (EcoChemie, The Netherlands) run by PCs with GPES software. Voltammograms were recorded for each substrate at a concentration of 7.5×10^{-4} M, at scan rates typically ranging from 0.05 to 2 V s^{-1}, after carefully compensating the ohmic drop by the positive feedback technique. The GPES software was used to carry out semi-integral analysis of the current recorded in linear sweep voltammetry.

The working electrodes were disks of glassy carbon (GC, Sigradur, geometric area = 0.033 cm^2), Au (geometric area = 0.031 cm^2) and Ag (geometric area = 0.071 cm^2). They were all purchased from AMEL and cleaned by polishing with a diamond powder (Aldrich, diameter 1 μm) on a wet cloth (DP-Nap, Struers).

The reference electrode was an aqueous saturated calomel electrode (SCE) inserted in a double bridge filled with the working medium to avoid diffusion of water and chloride anions into the working compartment, except when n-butanol was used as solvent. In this case, the reference electrode was put directly in solution, and the experiment was carried out rapidly to minimize the contact time. The counter electrode was a platinum wire.

The CV patterns recorded in different solvents were made comparable by intersolvental normalization of the corresponding potentials *vs* the $Fc^+|Fc$ reference couple, used as internal reference system. At the end of each experiment, the formal potential of $Fc^+|Fc$ versus SCE was measured in a separate cell containing only the background electrolyte and then all potentials were converted to the ferrocene scale, according to the IUPAC recommended procedure [40].

3. Results and discussion

Analysis of the voltammetric peak morphology and scan-rate dependence affords a valuable means of discriminating between DET mechanisms [3]. In particular, a diagnostic parameter κ can be calculated from the half-peak width or from the slope of the linear variation of E_p as a function of log v:

$$\kappa = -1.857 \frac{RT}{F(E_\mathrm{p} - E_\mathrm{p/2})} = -\frac{0.0477}{E_\mathrm{p} - E_\mathrm{p/2}}\,\mathrm{V} \qquad \text{at } 298\ \mathrm{K} \qquad (4)$$

$$\kappa = -1.151 \frac{RT}{F\partial E_\mathrm{p}/\partial \log \upsilon} = -\frac{0.0296}{\partial E_\mathrm{p}/\partial \log \upsilon}\,\mathrm{V} \qquad \text{at } 298\ \mathrm{K} \qquad (5)$$

In stepwise mechanism, κ lies between 0.5 and 1 if the process is under a mixed kinetic regime (ET and bond rupture have comparable energy barriers) or is kinetically controlled by the bond rupture. If, instead, ET is the rate-determining step, then $\kappa < 0.5$ and coincides with the transfer coefficient α. In this case, however, α often lies close to 0.5, since the reduction potential is near the standard potential. Equations (4) and (5) give also $\kappa = \alpha < 0.5$ when the reaction follows a concerted mechanism. In this case, the reaction has a very high intrinsic barrier resulting from the contribution of bond breaking, and consequently the reduction potential is considerably more negative than the standard potential and α is much below 0.5. These guidelines will be used to discriminate between concerted and stepwise mechanisms for the reductive cleavage of the model compounds in both protic and aprotic solvents. However, in some cases the peak shape on catalytic electrodes was affected by adsorption phenomena, precluding the use of equations (4) and (5), which are valid for a process under diffusion control. In such cases the parameter κ was not determined.

The catalytic effects on Ag and Au, ΔE_p, will be evaluated as the difference between peak potentials recorded on the catalytic electrode considered and on GC taken as a non-catalytic reference system, that is $\Delta E_\mathrm{p} = E_\mathrm{p,M} - E_\mathrm{p,GC}$. When more than one reduction peak was observed as in the case of haloanthracenes (ArX), the first peak was attributed to the reduction of the carbon-halogen bond. This was achieved by comparing cyclic voltammetry of anthracene (ArH) with that of ArX. In all cases, the voltammetric pattern of ArH was found to overlap that of ArX, if the first peak of the latter is excluded, clearly indicating that reduction of ArX at the first peak involves the C-X bond and generates ArH. Therefore, in these cases, only the first reduction peak of ArX was analysed.

3.1 CV features and DET mechanism for aliphatic halides

Haloacetonitriles CAN and BAN have been chosen as representatives of aliphatic halides, which typically undergo a concerted DET to give $R^{\bullet}$ and X^{-} [41-43]. The reduction potential of $NCCH_2^{\bullet}$ is more positive than E_p of $NCCH_2X$ [44], thus the overall process is a $2e^{-}$ reduction leading to $NCCH_2^{-}$ and X^{-}. In aprotic solvents, however, the charge consumption is often less than $2e^{-}$/molecule because of the presence of a father-son reaction (self-protonation) between $NCCH_2^{-}$ and $NCCH_2X$ [45,46].

$$NCCH_2X + NCCH_2^{-} \rightleftharpoons CH_3CN + NCCHX^{-} \qquad (6)$$

Reaction (6) can be suppressed by addition of a proton donor stronger than $NCCH_2X$. Figure 2 shows examples of the effect of acetic acid on the cyclic voltammetry of $NCCH_2X$. Addition of CH_3COOH almost doubles the peak height without significantly affecting E_p in aprotic solvents, whereas no appreciable effect was observed in protic solvents, indicating the absence of self-protonation (ROH is a better proton donor than $NCCH_2X$). Therefore, all voltammetric investigations on $NCCH_2X$ in aprotic solvents were performed in the presence of acetic acid. Figures 3 and 4 show synopses of voltammetric features of

CAN and BAN recorded on different electrodes in all solvents and the corresponding key parameters are collected in Table 2. In all solvents, a single bielectronic irreversible peak is observed on all electrodes. Analysis of the effect of scan rate on E_p and E_p - $E_{p/2}$, according to equations (4) an (5), gives α values significantly smaller than 0.5, in line with the well-established concerted nature of the dissociative electron transfer to alkyl halides [10,16,18]. In some solvents, cyclic voltammetry of $NCCH_2X$ at the catalytic electrodes, especially Ag, has shown voltammograms with adsorption peaks (see Fig. 4). Since in such cases the diagnostic criteria based on α, which was not measured, could not be used to discriminate between the two DET mechanisms, we simply assumed a concerted mechanism in analogy with the results obtained with the other solvents and electrodes.

Therefore, the overall reduction process underlying the observed single peak can be written as:

$$NCCH_2X + e^- \longrightarrow NCCH_2^\bullet + X^- \tag{7}$$

$$NCCH_2^\bullet + e^- \rightleftharpoons NCCH_2^- \tag{8}$$

$$NCCH_2^- + HOAc \rightleftharpoons CH_3CN + OAc^- \tag{9}$$

In all solvents E_p of BAN on GC is 0.25-0.3 V more positive than that of CAN; this feature is consistent with the alkyl bromide reduction being both thermodynamically and kinetically more favoured than that of the corresponding chloride, owing to the weaker carbon-halogen bond in BAN than in CAN [47]. On Au and Ag, the effect of the halide leaving group still remains, but the reduction potentials are remarkably shifted in the positive direction with respect to GC, emphasizing the catalytic nature of the process at these metallic electrodes. The catalytic activity, quantified as the difference between the peak potentials measured at GC and each metal, $\Delta E_p = E_{p,M} - E_{p,GC}$, is reported in Table 2. In all solvents, Ag shows considerably higher catalytic activities than Au. This can be justified, as mentioned in the introduction, considering that Au, albeit being potentially more catalytic than Ag [23,24] has a much more positive PZC than Ag [24,25]). In the potential range typical of RX reduction, the Au surface bears a large negative charge, which considerably decreases the affinity of the metal for X^-. In contrast, Ag does not suffer from this setback and fully manifests its catalytic activities.

The CV synopses on all electrodes evidence a strong dependence of the current on solvent. This effect is due to variations of solvent viscosity, η, which affect the mass transport to and from the electrode, through the Stokes-Einstein equation:

$$D = \frac{k_B T}{6\pi\eta a} \tag{10}$$

where k_B is the Boltzmann constant and a is the hydrodynamic radius of the diffusing species. Semi-integration of the current in the negative-going scan of cyclic voltammetry converts the peak-shaped curve to an S-shaped one with a limiting current given by [48]:

$$I_L = nFACD^{1/2} \tag{11}$$

where *n* is the number of electrons exchanged, *A* is the area of the electrode and *C* is the bulk concentration of the electroactive species. Equations (10) and (11) can be combined to show that I_L decreases with increasing viscosity, and, if all other parameters are kept constant, I_L should vary linearly with $\eta^{-1/2}$. Plots of I_L vs. $\eta^{-1/2}$ have shown fairly straight lines for both catalytic and non-catalytic electrodes in different solvents. This suggests that in the case of the catalytic surfaces, although certainly adsorption phenomena play a crucial role, the overall process can be considered to occur under diffusion control, which means adsorption/desorption processes involving reagents, intermediates and products are quite fast. This is also confirmed by plots of I_P vs $\upsilon^{1/2}$, which are straight lines in all solvents and on all electrodes, typical of an electrode process under diffusion control. It is, however, important to stress that some CV features indicative of adsorption phenomena were observed in several cases on the catalytic electrodes (Figs. 3-4).

3.2 CV features and DET mechanism for haloanthracenes in aprotic solvents

The CV features of 9-chloro- and 9-bromoanthracene in the investigated eight solvents are shown in Figures 5 and 6, whereas the key voltammetric data are reported in Table 3. The first cathodic peak is attributed to the reductive cleavage of the C-X bond; it is irreversible in the whole range of scan-rates examined. As in the case of haloacetonitriles, the current intensity of CA and BA reduction varies strongly with the solvent, increasing with decreasing solvent viscosity. Plots of I_L versus $\eta^{-1/2}$ show roughly linear variations. Also plots of I_P versus $\upsilon^{1/2}$ give straight lines, indicating an overall reduction process under diffusion control.

In all aprotic solvents, both haloanthracenes exhibit a second reversible peak, which is attributed to the one-electron reduction of anthracene to a relatively stable aromatic radical anion:

$$\mathrm{ArH} + e^{-} \rightleftharpoons \mathrm{ArH}^{\bullet -} \tag{12}$$

The peak potentials measured for this process slightly vary with solvent but do not depend on the nature of the electrode. Since reduction of anthracene does not involve rupture of a carbon-halogen bond and is electrochemically reversible, no catalytic effects were observed on Ag or Au.

In all aprotic solvents, both CA and BA show κ values well above 0.5, clearly indicating a stepwise mechanism.

$$\mathrm{ArX} + e^{-} \rightleftharpoons \mathrm{ArX}^{\bullet -} \tag{13}$$

$$\mathrm{ArX}^{\bullet -} \longrightarrow \mathrm{Ar}^{\bullet} + \mathrm{X}^{-} \tag{14}$$

The aryl radical $\mathrm{Ar}^{\bullet}$ undergoes fast reduction at the electrode or in solution by $\mathrm{ArX}^{\bullet -}$ to give a carbanion that rapidly reacts with any proton donor, HA, present in solution to form the hydrodehalogenated aromatic derivative, which in our case is anthracene:

$$\mathrm{Ar}^{\bullet} + e^{-} \rightleftharpoons \mathrm{Ar}^{-} \tag{15}$$

$$\mathrm{Ar}^{\bullet} + \mathrm{ArX}^{\bullet -} \rightleftharpoons \mathrm{Ar}^{-} + \mathrm{ArX} \tag{16}$$

$$\mathrm{Ar^- + HA \rightleftharpoons ArH + A^-} \quad (17)$$

$\mathrm{Ar^\bullet}$ may also abstract a hydrogen atom from the solvent and thus trigger a series of radical reactions [49,50]. The overall charge consumption, n (e^-/molecule), of the process therefore depends on a blend of radical and anionic reactions that are strongly affected by the reaction medium. To evaluate n we compared the convoluted limiting current of the DET process with that of the one-electron reduction of anthracene. If one assumes similar diffusion coefficients for anthracene and 9-haloanthracene, n can be estimated as $n = I_L(\mathrm{ArX})/I_L(\mathrm{ArH})$, where ArX and ArH stand for 9-haloanthracene and anthracene, respectively. For both haloanthracenes, n values well below 2, with average values of 1.28 and 1.36 for CA and BA, respectively, were obtained in all aprotic solvents, indicating complex overall reduction processes.

As shown in Table 3, in all aprotic solvents E_p of BA is *ca* 0.1 V more positive than that of CA, independently of the nature of the electrode material. It is important to note that a significantly bigger difference has been observed between the peak potentials of the two alkyl halides CAN and BAN. In contrast to the aliphatic halides, aromatic halides give rise to an intermediate radical anion in which both the negative charge and the spin density are delocalized in the whole molecule. Therefore, the halogen atom only slightly affects the standard potential, also because Cl and Br have similar polar effects [51]. A major difference between the two aromatic radical anions is their stability, the cleavage rate of $\mathrm{ArBr^{\bullet-}}$ being *ca* 4 orders of magnitude higher than that of $\mathrm{ArCl^{\bullet-}}$ [50]. Since reduction of ArX is a reversible ET followed by an irreversible chemical reaction, E_p is positively shifted with respect to $E^{\ominus}$ and the extent of this shift depends on the rate constant of the chemical reaction. It is therefore likely that the observed difference in the peak potentials of the two haloanthracenes arises from this kinetic effect.

3.3 CV features and DET mechanism of aryl halides in protic solvents

In protic solvents a remarkable change is observed in the voltammetric pattern of 9-haloanthracenes even under non-catalytic conditions, *i.e.*, on GC. In particular, the second reduction peak becomes chemically irreversible; moreover, in the case of BA, the second peak has roughly the same height of the first peak, suggesting that the two reduction processes have now comparable charge consumption (Figs. 5-6).

To explain these changes we assume the mechanism represented in Scheme 1 for BA, where (a) and (b) stand for the reaction sequences underlying the first and second peaks, respectively. The first cathodic process involves two-electron reduction of ArX to give ArH, which is further reduced at the second peak. In this case, however, owing to the high proton availability in the medium, the radical anion $ArH^{\bullet-}$ is rapidly protonated, triggering a sequence of ET and proton transfers resulting in a chemically irreversible bielectronic peak. It is known that aromatic hydrocarbons exhibit a $2e^{-}$ reduction peak (or wave) in protic solvents or in aprotic solvents with added proton donors [52].

Also in the CA case the first reduction peak is followed by a second irreversible peak, attributed to the reduction of anthracene. However, the CV pattern of CA significantly differs from that of BA. In all protic solvents, the first peak is always higher than the second one; the

I_p(I)/I_p(II) ratio increases with decreasing pK_a of ROH, *i.e.* increases from n-BuOH to MeOH. It appears that less and less anthracene is produced at the first reduction peak of CA as the acidity of the solvent increases. The reduction mechanism of CA is more complicated than that of BA and presents other unknown reaction pathways, possibly initiated by protonation of the CA radical anion, in competition with the hydrodehalogenation sequence reported in Scheme 1a. Dehalogenation of BA radical anion ($BA^{\bullet-}$) is about 4 orders of magnitude faster than that of CA radical anion ($CA^{\bullet-}$) [50]. It is therefore possible that protonation of $CA^{\bullet-}$ becomes competitive with dehalogenation in protic solvents, and more so as pKa of the solvent decreases, whereas it is irrelevant in the case of $BA^{\bullet-}$ ($k_d \approx 10^6$ s^{-1} [50]).

No reduction peaks were observed on Au, because the process on this electrode is overshadowed by the cathodic solvent discharge. Also on Ag the accessible potential window becomes smaller with respect to GC, but in this case a single irreversible cathodic peak due to the reduction of C–X was observed for both haloanthracenes (Figs. 5 and 6). Again, reduction of anthracene is covered by the cathodic solvent discharge. Although we were not able to check whether and to what extent anthracene is formed at Ag, we assume the same reaction mechanisms previously discussed in the case of GC cathode.

The values of E_p measured at GC and Ag in all four protic solvents are included in Table 3. However, the voltammetric data were analysed according to equations (4) and (5) only in the case of 9-bromoanthracene for which an ECE/DISP reduction mechanism is assumed. Considering the complexity of the reduction process of 9-chloroanthracene, we made no attempts to distinguish between concerted and stepwise DET mechanisms. As shown in Table 3, reduction of BA at GC and Ag in the protic solvents is characterised by κ values greater than or only slightly smaller than 0.5, clearly indicating a stepwise mechanism. κ was not evaluated for CA reduction, but we may assume a stepwise mechanism since a change of mechanism from stepwise to concerted is quite unlikely when the leaving group is changed from bromide to chloride [2].

3.4 Surface effects on aryl halide reduction

No catalytic effect was observed on the Au surface in aprotic solvents, whereas the catalytic activity in protic solvents could not be measured because of a strong positive shift of the cathodic limit to potentials more positive than the reduction potential of ArX. Conversely, Ag exhibits remarkable electrocatalytic activities for the reduction of both halides. In all solvents, peak potentials of BA at Ag were significantly shifted to more positive values with respect to GC, whereas a positive shift of E_P was observed only in protic solvents in the case of CA. Quite interestingly, the general observation that this metal does not show catalytic effects for the reduction of aryl chlorides [18, 53] holds in aprotic solvents but not in protic ones.

3.5 Reduction potential and primary medium effect

Aiming to rationalize the solvent dependence of peak potentials and catalytic effects, we have considered the primary medium effect (PME), $\gamma_{t\,(X^-,\,W\rightarrow S)}$, a quantity related to the standard Gibbs energy of transfer of an anion X^- from infinite dilution in water to infinite dilution in solvent S:

$$\log \gamma_{t\,(X^-,\,W\rightarrow S)} = \Delta G_t^\circ{}_{(X^-,\,W\rightarrow S)} \,/\, (2.303\,RT) \qquad (18)$$

This quantity is positive if the solvation of X^- is stronger in water than in S, whereas it is negative if the opposite is true. PME is perhaps the most convenient parameter to rationalize phenomena depending on ion solvation, because of its "integral" nature, concurrently accounting for all possible factors involved in solvation, such as relative permittivity, viscosity, autoprotolysis constant, dipole moment, *etc*. In other words, it can be conveniently used to account for solvation effects without the need of developing solvation models. Furthermore, it is of experimental origin, which makes it quite reliable.

PME values for Cl^- and Br^- anions in the solvents considered in this work are reported in Table 1 [39]. The four aprotic solvents have more positive $\log\gamma_{t\,(X^-,\,W\rightarrow S)}$ values than the alcohols, implying lower ability for halide anion solvation; in turn, in the alcohol series, $\log\gamma_{t\,(X^-,\,W\rightarrow S)}$ regularly decreases (and the halide solvation ability increases) from BuOH to MeOH, which also coincides with increasing order of proticity.

In Fig. 7, E_p values measured *vs* $Fc^+|Fc$ for all four halides are plotted versus the primary medium effects for the corresponding halide leaving groups, $\log\gamma_{t\,(X^-,\,W\rightarrow S)}$. The horizontal lines in the figure stand for the estimated threshold for halide ion specific adsorption on Ag [30,31]. In fact, we have often noticed that the potential range in which adsorption processes are taking place not only affects the peak morphology (introducing features typical of adsorption peaks, as for the bromoacetonitrile case, Fig. 4) but also sets a kind of threshold to the catalytic effects that can be obtained on the Ag electrode. Interestingly, in nearly all cases it looks as if two neatly independent series were plotted together (evidenced by the vertical dotted line), one corresponding to the aprotic solvents and the other to the protic ones.

In particular, solvent effects are hardly perceivable in the aprotic solvent series. A slight positive trend with increasing anion solvation ability might be observed for the reduction of CAN, CA and BA, but not in the case of BAN, possibly because the process is strongly affected by adsorption phenomena, falling well before the bromide adsorption threshold. Instead, in the alcohol series, reduction potentials neatly and regularly shift to more positive values in the sequence: BuOH < PrOH < EtOH < MeOH. Since such a sequence corresponds to both decreasing PMEs (*i.e.*, increasing solvation ability for the halide leaving groups) and increasing proticity, both features should be taken into account for interpretative purposes. In this light, a further useful observation is that such a positive shift of E_p in the protic solvent series is observed (a) only on catalytic electrodes for concerted DETs, (b) on both types of electrode for stepwise DETs, particularly in the CA case, where neatly parallel characteristics are observed on Ag and GC, while such dependence is less marked on GC in the BA case.

This might suggest that in the case of concerted DET, in which the electron transfer is kinetically determining, protic solvent effects could particularly be related to the catalytic surface activity, for instance in terms of enhanced regeneration of the catalytic sites from adsorbed reaction products, as a consequence of both enhanced protonation of adsorbed R^- [34] and enhanced solvation of adsorbed X^- . On the other hand, in the case of stepwise DET, in which the rds is the chemical evolution of the radical anion, the solvent effects should be related more to the intrinsic reactivity of the molecule, which might be enhanced by both solvation of the halide leaving group and protonation of the radical anion; in this light, the neater E_p *vs* log $\gamma_{t\,(X^-,\,W\rightarrow S)}$ trend observed for CA with respect to BA would appear consistent with the higher relevance of protonation for CA radical anion with respect to the radical anion of BA, as discussed in the previous section.

3.6 Catalytic surface activity

Figure 8 compares catalytic surface effects, $E_{p,M} - E_{p,GC}$, plotted *vs* the primary medium effects for the corresponding halide leaving groups, log$\gamma_{t\,(X-,\,W\rightarrow S)}$. Consistently with former observations [18], catalytic effects appear remarkably higher when DET follows a concerted mechanism than a stepwise one. However, in all cases the catalytic effects at both Ag and Au electrodes are much higher in protic solvents than in aprotic solvents. Actually, significant enhancements of the catalytic activities of metals such as Ag and Cu in the presence of proton donors [12,34,37,54] or electrophiles such as CO_2 [55] have been previously reported; in particular, these species have been assumed to modify the reaction kinetics by acting as rapid scavengers of adsorbed carbanions formed during the reductive cleavage of RX [34].

It is, however, worthwhile noticing that all the above studies refer to alkyl or benzyl halides, which always undergo concerted DET. In this light the present work, while confirming such observations and generalizing them in a whole solvent series, also affords an interesting comparative evaluation of the reductive cleavage of aryl halides, undergoing a stepwise DET.

In the case of concerted DETs, catalytic effects regularly increase in the alcohols with both PME (Fig. 8) and proticity (Fig. 9), consistently with the above mechanistic assumptions about the scavenger role of proton donors for catalytic sites regeneration. It is worthwhile noticing that such an increase is steeper for BAN than for CAN (this is particularly evident in Fig. 9); this is consistent with BAN reduction taking place at less negative potentials, where the negative charge density on the electrode is lower and therefore the adsorption of negatively charged species is higher.

For stepwise DETs, catalytic effects appear constant with both PME (Fig. 8) and alcohol pK_a (Fig. 9). As discussed above, this could be justified assuming that in this case solvent effects influence the intrinsic molecular reactivity rather than the catalytic surface activity, and therefore the solvent has almost the same effect on catalytic and non-catalytic electrodes, so that catalytic effects are constant.

In any case, it is very important to observe that catalytic effects are observed on Ag for the first time in protic media for aryl chlorides, which are totally unaffected by silver electrocatalysis in aprotic solvents [53].

Finally, as already mentioned, lower catalytic effects are observed on Au with respect to Ag, on account of its much more negative specific surface charge [22-24,37]. It is interesting to notice that whereas on silver lower catalytic effects are observed for BAN with respect to CAN, possibly on account of significant surface screening by adsorbed bromides at the working potential, the opposite is true for Au, where such adsorption cannot take place on account of the much more negative surface charge in the same potential range. No catalytic effect was observed on Au for the reduction of CA and BA in aprotic solvents, whereas the catalytic effect in alcohols could not be evaluated as the reduction process in these solvents occurs beyond the cathodic background discharge.

4. Conclusions and perspectives

An exhaustive study has been carried out on the effect of solvent on the reductive cleavage of carbon-halogen bonds for two aromatic and two alkyl halides, forming a set of RX that is representative of chlorides and bromides as well as both DET mechanisms. The process was investigated on both non–catalytic GC and catalytic Ag and Au electrodes.

In all solvents, remarkable catalytic effects were observed for the reduction of the alkyl halides, which undergo reduction according to a concerted DET mechanism, as already observed in acetonitrile [18]. On Au, albeit being intrinsically more catalytic than Ag, the observed catalytic effects were lower than on Ag, consistently with the high negative specific charge on Au surface in the operating potential range.

The most striking observation is that solvent proticity deeply affects both the reaction mechanism (on both non-catalytic and catalytic electrode surfaces) and the extent of the catalytic effects. In particular, in concerted DET cases a high enhancement is observed for catalytic effects in protic solvents, regularly increasing with solvent proticity, possibly connected with increasing efficiency of catalytic sites turnover, consistently with former literature observations. In stepwise DET cases, significant catalytic effects were also observed in all protic solvents. This is a particularly interesting result emphasizing that electrocatalytic reduction of aromatic chlorides on Ag is possible in protic solvents.

Acknowledgements

This work was financially supported by University of Milan and University of Padova.

References

[1] D.G. Peters, Halogenated organic compounds, in: H. Lund, O. Hammerich (Eds), Organic Electrochemistry, 4th ed., Marcel Dekker, New York, 2001, Ch. 8.

[2] J.-M. Savéant, Elements of Molecular and Biomolecular Electrochemistry, Wiley, New Jersey, 2006, Ch. 3.

[3] A.A. Isse, P.R. Mussini, A. Gennaro, New insights into electrocatalysis and dissociative electron transfer mechanisms: The case of aromatic bromides, J. Phys. Chem. C 113 (2009) 14983.

[4] J. Simonet, The one electron reduction of primary alkyl iodides at palladiated surfaces. A convenient and general source of alkyl radicals, J. Electroanal. Chem. 583 (2005) 34.

[5] J. Simonet, The copper–palladium cathode to achieve pure one-electron cleavages: The case of alkyl bromides, Electrochem. Commun. 7 (2005) 619.

[6] P. Poizot, J. Simonet, Silver-palladium cathode: Selective one-electron scission of alkyl halides: Homo-coupling and cross-coupling subsequent reactions, Electrochim. Acta 56 (2010) 15.

[7] J. Simonet, Gold doped by palladium: Building of Au-Pd electrodes showing exceptional capability for achieving electrocatalytic reductions, Electrochem. Commun. 12 (2010) 1475.

[8] P. Poizot, O. Durand-Drouhin, M. Lejeune, J. Simonet, Changes in a glassy carbon surface by the cathodic generation of free alkyl radicals mediated by a silver-palladium catalyst, Carbon, 50 (2012) 73.

[9] C. Durante, V. Perazzolo, A.A. Isse, M. Favaro, G. Granozzi, A. Gennaro, Electrochemical activation of carbon halogen bonds: Electrocatalysis at palladium/copper nanoparticles, ChemElectroChem 1 (2014) 1370.

[10] A.A. Isse, S. Gottardello, C. Durante, A. Gennaro, Dissociative electron transfer to organic chlorides: Electrocatalysis at metal cathodes, Phys. Chem. Chem. Phys. 10 (2008) 2409.

[11] B. Huang, A.A. Isse, C. Durante, C. Wei, A. Gennaro, Electrocatalytic properties of transition metals towards reductive dechlorination of polychloroethanes, Electrochim. Acta 70 (2012) 50.

[12] C. Durante, B. Huang, A.A. Isse, A. Gennaro, Electrocatalytic dechlorination of volatile organic compounds at a copper cathode. Part II: Polychloroethanes, Appl. Catal. B: Environ. 126 (2012) 355.

[13] J. Langmaier, Z. Samec, Electrocatalytic reduction of halothane, J. Electroanal. Chem. 402 (1996) 107.

[14] C. Bellomunno, D. Bonanomi, L. Falciola, M. Longhi, P.R. Mussini, L. M. Doubova, G. Di Silvestro, Building up an electrocatalytic activity scale of cathode materials for organic halide reduction, Electrochim. Acta 50 (2005) 2331.

[15] S.B. Rondinini, P.R.Mussini, P. Muttini, G. Sello, Silver as a powerful electrocatalyst for organic halide reduction: The critical role of molecular structure, Electrochim. Acta 46 (2001) 3245.

[16] A.A. Isse, A. De Giusti, A. Gennaro, L. Falciola, P.R. Mussini, Electrochemical reduction of benzyl halides at a silver electrode, Electrochim. Acta 51 (2006) 4956.

[17] A.A. Isse, A. De Giusti, A. Gennaro, One- versus two-electron reaction pathways in the electrocatalytic reduction of benzyl bromide at silver cathodes, Tetrahedron Lett. 47 (2006) 7735.

[18] A.A. Isse, G. Berzi, L. Falciola, M. Rossi, P.R. Mussini, A. Gennaro, Electrocatalysis and electron transfer mechanisms in the reduction of organic halides at Ag, J. Appl. Electrochem. 39 (2009) 2217.

[19] A.A. Isse, G. Sandonà, C. Durante, A. Gennaro, Voltammetric investigation of the dissociative electron transfer to polychloromethanes at catalytic and non-catalytic electrodes, Electrochim. Acta 54 (2009) 3235.

[20] A. Ignaczak, J.A.N.F. Gomes, Quantum calculations on the adsorption of halide ions on the noble metals, J. Electroanal. Chem. 420 (1997) 71.

[21] M.T.M. Koper, R.A. van Santen, Interaction of halogens with Hg, Ag, and Pt surfaces: a density functional study, Surf. Sci. 422 (1999) 118.

[22] G. Valette, Energies involved in the specific adsorption of halides on sd metals. Part I. Analysis of experimental results, J. Electroanal. Chem. 255 (1988) 215.

[23] G. Valette, Energies involved in the specific adsorption of halides on sd metals. Part II. Parallelism with energies involved in the formation of the corresponding bulk compounds and comparison with sp metals, J. Electroanal. Chem. 255 (1988) 225.

[24] A. Hamelin, Modern Aspects of Electrochemistry in: B.E. Conway, R.E. White, J. O'M.Bockris (Eds.), Vol. 16, Ch. 6, Plenum Press, New York, 1985.

[25] S. Trasatti, Prediction of double layer parameters. The case of silver, J. Electroanal. Chem. 172 (1984), 27.

[26] A. Wang, Y.-F. Huang, U. K. Sur, D.-Y. Wu, B. Ren, S. Rondinini, C. Amatore, Z.-Q. Tian, In Situ identification of intermediates of benzyl chloride reduction at a silver electrode by SERS coupled with DFT calculations, J. Am. Chem. Soc. 132 (2010) 9534.

[27] Y.-F. Huang, D.-Y. Wu, A. Wang, B. Ren, S. Rondinini, Z.-Q. Tian, C. Amatore, Bridging the gap between electrochemical and organometallic activation: benzyl chloride reduction at silver cathodes, J. Am. Chem. Soc. 132 (2010) 17199.

[28] O. V. Klymenko, O. Buriez, E. Labbe, D.-P. Zhan, S. Rondinini, Z.-Q. Tian, I. Svir, C. Amatore, Uncovering the missing link between molecular electrochemistry and electrocatalysis: mechanism of the reduction of benzyl chloride at silver cathodes, ChemElectroChem 1 (2014) 227.

[29] S. Ardizzone, G. Cappelletti, L.M. Dou bova, P. R. Mussini, S.M. Passeri, S. Rondinini, The role of surface morphology on the electrocatalytic reduction of organic halides on mono- and polycrystalline silver, Electrochim. Acta 48 (2003) 3789.

[30] S. Ardizzone, G. Cappelletti, P.R. Mussini, S. Rondinini, L.M. Doubova, Adsorption competition effects in the electrocatalytic reduction of organic halides on silver, J. Electroanal. Chem. 532 (2002) 285.

[31] L. Falciola, P.R. Mussini, S. Trasatti, L.M. Doubova, Specific adsorption of bromide and iodide anions from nonaqueous solutions on controlled-surface polycrystalline silver electrodes, J. Electroanal. Chem. 593 (2006) 185.

[32] A. Gennaro, A.A. Isse, E. Giussani, P.R. Mussini, I. Primerano, M. Rossi, Relationship between supporting electrolyte bulkiness and dissociative electron transfer at catalytic and non-catalytic electrodes, Electrochim. Acta 89 (2013) 52.

[33] L. Falciola, A. Gennaro, A.A. Isse, P.R. Mussini, M. Rossi, The solvent effect in the electrocatalytic reduction of organic bromides on silver, J. Electroanal. Chem. 593 (2006) 47.

[34] O. Lugaresi, A. Minguzzi, C. Locatelli, A. Vertova, S. Rondinini, C. Amatore, Benzyl chloride electroreduction on Ag cathodes in CH_3CN in the presence of small amounts of water: Evidences of quantitative effects on reaction rates and mechanism, Electrocatalysis 45 (2013) 353.

[35] A.B. Pierini, D.M. Vera, Ab initio evaluation of intramolecular electron transfer reactions in halobenzenes and stabilized derivatives, J. Org. Chem. 68 (2003) 9191.

[36] L. Pause, M. Robert, J.-M. Savéant, Stabilities of ion/radical adducts in the liquid phase as derived from the dependence of electrochemical cleavage reactivities upon solvent, J. Am. Chem. Soc. 123 (2001) 11908.

[37] M. Fedurco, C.J. Sartoretti, J. Augustynski, Medium effects on the reductive cleavage of the carbon-halogen bond in methyl and methylene halides, J. Phys. Chem. B 105 (2001) 2003.

[38] A. Gennaro, A.A. Isse, C.L. Bianchi, P.R. Mussini, M. Rossi, Is glassy carbon a really inert electrode material for the reduction of carbon-halogen bonds?, Electrochem. Commun. 11 (2009) 1932.

[39] K. Izutsu, Electrochemistry in Nonaqueous Solutions, Second, Revised and Enlarged Edition Wiley-VCH, Weinheim, 2009, and references cited therein.

[40] G. Gritzner, J. Kuta, Recommendations on reporting electrode potentials in nonaqueous solvents, Pure Appl. Chem. 56 (1984) 461.

[41] C.P. Andrieux, I. Gallardo, J.-M. Savéant, K.B. Su, Dissociative electron transfer. Homogeneous and heterogeneous reductive cleavage of the carbon-halogen bond in simple aliphatic halides, J. Am. Chem. Soc. 108 (1986) 638.

[42] W. Adcock, C.I. Clark, A. Houmam, A.R. Kristic, J. Pinson, J.-M. Savéant, D.K. Taylor, J.F. Taylor, Dissociative electron transfer to dihaloalkanes. Electrochemical reduction of 1,3-dihaloadamantanes, 1,4-dihalobicyclo[2.2.2]octanes, and 1,3-dihalobicyclo[1.1.1]pentanes, J. Am. Chem. Soc. 116 (1994) 4653.

[43] A. Cardinale, A.A. Isse, A. Gennaro, M. Robert, J.-M. Savéant, Dissociative electron transfer to haloacetonitriles. An example of the dependency of in-cage ion-radical interaction upon the leaving group, J. Am. Chem. Soc. 124 (2002) 13533.

[44] N. Bortolamei, A.A. Isse, A. Gennaro, Estimation of standard reduction potentials of alkyl radicals involved in atom transfer radical polymerization, Electrochim. Acta 55 (2010) 8312.

[45] A.A. Isse, A. Gennaro, Electrochemical synthesis of cyanoacetic acid from chloroacetonitrile and carbon dioxide, J. Electrochem. Soc. 149 (2002) D113.

[46] O. Scialdone, A. Galia, G. Filardo, A.A. Isse, A. Gennaro, Electrocatalytic carboxylation of chloroacetonitrile at a silver cathode for the synthesis of cyanoacetic acid, Electrochim. Acta 54 (2008) 634.

[47] A.A. Isse, C.Y. Lin, M.L. Coote, A. Gennaro, Estimation of standard reduction potentials of halogen atoms and alkyl halides, J. Phys. Chem. B 115 (2011) 678.

[48] A.J. Bard, L.R. Faulkner, Electrochemical Methods. Fundamentals and Applications, Wiley, New York, 2001, p. 247.

[49] F. M'Halla, J. Pinson, J.-M. Savéant, The solvent as hydrogen-atom donor in organic electrochemical reactions. Reduction of aromatic halides, J. Am. Chem. Soc. 102 (1980) 4120.

[50] C.P. Andrieux, J.-M. Savéant, D. Zann, Relationship between reduction potentials and anion radical cleavage rates in aromatic molecules, Nouv. J. Chim. 8 (1984) 107.

[51] C. Hansch, A. Leo, R.W. Taft, A survey of Hammett substituent constants and resonance and field parameters, Chem. Rev. 91 (1991) 165.

[52] J. Heinze, Cathodic reactions of hydrocarbons, in H. Lund, O. Hammerich, eds, Organic Electrochemistry, 4th ed., Marcel Dekker, New York, 2001, p. 306.

[53] A.A. Isse, L. Falciola, P.R. Mussini, A. Gennaro, Relevance of electron transfer mechanism in electrocatalysis: The reduction of organic halides at silver electrodes, Chem. Commun. 3 (2006) 344.

[54] O. Scialdone, C. Guarisco, A. Galia, R. Herbois, Electroreduction of aliphatic chlorides at silver cathodes in water, J. Electroanal. Chem. 641 (2010) 14.

[55] A.A. Isse, A. Gennaro, Electrocatalytic carboxylation of benzyl chlorides at silver cathodes in acetonitrile, Chem. Commun. (2002) 2798.

Figure captions

Figure 1. The rationale for the model halide selection.

Figure 2. Cyclic voltammetry of 7.5×10^{-4} M $NCCH_2X$ recorded on GC in (a) DMF + 0.1 M n–Bu_4NBF_4 or (b) n-BuOH + 0.1 M n–Bu_4NBF_4 in the absence (—) and presence (— —) of 1.5×10^{-3} M acetic acid; $v = 0.2$ V/s.

Figure 3. A synopsis of normalized CV patterns of chloroacetonitrile recorded at 0.2 V/s on GC (—·—), Au (— —) and Ag (—) in protic and aprotic solvents containing 0.1 M n–Bu_4NBF_4.

Figure 4. A synopsis of normalized CV patterns of bromoacetonitrile recorded at 0.2 V/s on GC (—·—), Au (— —) and Ag (—) in protic and aprotic solvents containing 0.1 M n–Bu_4NBF_4.

Figure 5. A synopsis of normalized CV patterns of 9-chloroanthracene recorded at 0.2 V/s on GC (—·—), Au (— —) and Ag (—) in protic and aprotic solvents containing 0.1 M n–Bu_4NBF_4.

Figure 6. A synopsis of normalized CV patterns of 9-bromoanthracene recorded at 0.2 V/s on GC (—·—), Au (— —) and Ag (—) in protic and aprotic solvents containing 0.1 M n–Bu_4NBF_4.

Figure 7. Solvent effects on the reduction peak potential of RX on GC (△), Au (□) and Ag (○).

Figure 8. Solvent effects on the catalytic activity of Au (□) and Ag (○) for the reduction of RX.

Figure 9. Proticity effect on the catalytic activity of Ag for the reduction of RX.

Scheme 1. Proposed reduction mechanism for 9-bromoanthracene in protic solvents on GC. (a) First reduction peak, (b) second reduction peak.

Table 1

Table 1. Physical and chemical proprieties of selected organic solvents.[a]

Solvent	Viscosity /cP	Relative permittivity	$\log\gamma_{\mathrm{t}\,(\mathrm{Cl}^-,\,\mathrm{W}\to\mathrm{S})}$[b]	$\log\gamma_{\mathrm{t}\,(\mathrm{Br}^-,\,\mathrm{W}\to\mathrm{S})}$[b]	pK_a
AC	0.303	20.6	10	7.4	≥ 32.5
DMF	0.802	36.7	8.5	6.4	≥ 31.6
MeCN	0.341	35.9	7.4	5.5	≥ 33.3
DMSO	1.990	46.5	7.1	4.8	33.3
n-BuOH	2.58 [c]	17.4 [c]	5.6 [c]	4.3 [c]	21.6
n-PrOH	1.943	20.5	4.6	3.9	19.43
EtOH	1.083	24.6	3.5	3.2	18.88
MeOH	0.551	32.7	2.3	1.9	17.20

[a] Data taken from Ref. [39].

[b] Primary medium effect ($\Delta G^{\ominus}_{\mathrm{t}(\mathrm{X}^-,\,\mathrm{W}\to\mathrm{S})}$) for the transfer of ions from water (W) to any solvent (S).

[c] Estimated through extrapolation of data pertaining to the ROH series.

Table 2

Table 2. Data for the reduction of haloacetonitriles in protic and aprotic solvents on different electrodes.[a]

		Chloroacetonitrile			Bromoacetonitrile		
Electrode	Solvent	E_p /V	α[b]	ΔE_p[c] /V	E_p /V	α[b]	ΔE_p[c] /V
GC	AC	-2.50	0.32		-2.06	0.36	
	DMF	-2.46	0.37		-2.03	0.38	
	MeCN	-2.49	0.32		-2.03	0.39	
	DMSO	-2.42	0.36		-1.98	0.37	
	n-BuOH	-2.46	0.17		-1.92	0.36	
	n-PrOH	-2.50	0.16		-1.93	0.34	
	EtOH	-2.41	0.23		-2.02	0.34	
	MeOH	-2.41	0.22		-2.02	0.36	
Au	AC	-2.15	0.17	0.35	-1.61	0.21	0.45
	DMF	-2.25	0.17	0.21	-1.52	0.22	0.51
	MeCN	-1.98	0.21	0.51	-1.58	0.22	0.45
	DMSO	-2.18	0.26	0.24	-1.66	0.18	0.32
	n-BuOH	-2.10	0.12	0.36	-1.70	0.19	0.22
	n-PrOH	-2.19	0.16	0.31	-1.64	0.19	0.29
	EtOH	-1.98	0.27	0.43	-1.56		0.46
	MeOH	-1.87	0.36	0.54	-1.27	0.28	0.75
Ag	AC	-1.71	0.38	0.79	-1.40		0.66
	DMF	-1.64	0.42	0.82	-1.35		0.68
	MeCN	-1.61	0.42	0.88	-1.40		0.63
	DMSO	-1.58	0.41	0.84	-1.47		0.51
	n-BuOH	-1.58	0.15	0.88	-1.46		0.46
	n-PrOH	-1.58	0.18	0.92	-1.25		0.68
	EtOH	-1.45	0.27	0.96	-1.22		0.80
	MeOH	-1.39	0.25	1.02	-1.16		0.86

[a] Supporting electrolyte: 0.1 M n-Bu_4BF_4; E_p (*vs* $Fc^+|Fc$) measured at $v = 0.2\ Vs^{-1}$.

[b] Average of the values derived from $E_p - E_{p/2}$ and $\partial E_p/\partial \log v$.

[c] $\Delta E_p = E_{p,M} - E_{p,GC}$, where $E_{p,M}$ and $E_{p,GC}$ are the peak potentials measured at M (Au or Ag) and GC, respectively.

Table 3

Table 3. Data for the reduction of 9-haloanthracenes in protic and aprotic solvents on different electrodes.[a]

		9-Chloroanthracene			9-Bromoanthracene		
Electrode	Solvent	E_p /V	κ[b]	ΔE_p[c] /V	E_p /V	κ[b]	ΔE_p[c] /V
GC	AC	-2.24	0.82		-2.09	0.94	
	DMF	-2.18	0.90		-2.07	0.85	
	MeCN	-2.18	0.87		-2.04	0.88	
	DMSO	-2.11	0.89		-1.99	0.86	
	n-BuOH	-2.46			-2.21	0.38	
	n-PrOH	-2.37			-2.09	0.68	
	EtOH	-2.32			-2.08	0.72	
	MeOH	-2.25			-2.05	0.64	
Au	AC	-2.24	0.88	0	-2.09	0.92	0
	DMF	-2.18	0.89	0	-2.08	0.89	-0.01
	MeCN	-2.18	0.81	0	-2.04	0.85	0
	DMSO	-2.12	0.84	-0.01	-2.00	0.74	-0.01
	n-BuOH						
	n-PrOH						
	EtOH						
	MeOH						
Ag	AC	-2.23	0.77	0.01	-1.85	0.77	0.24
	DMF	-2.18	0.86	0	-1.92	0.56	0.15
	MeCN	-2.17	0.83	0.01	-1.72	0.59	0.32
	DMSO	-2.12	0.87	-0.01	-2.01	0.67	-0.02
	n-BuOH	-1.95		0.51	-1.58	0.44	0.63
	n-PrOH	-1.86		0.51	-1.53	0.47	0.56
	EtOH	-1.79		0.53	-1.47	0.53	0.61
	MeOH	-1.73		0.52	-1.42	0.47	0.63

[a] Supporting electrolyte: 0.1 M $n\text{-Bu}_4\text{BF}_4$; E_p (vs $\text{Fc}^+|\text{Fc}$) measured at $v = 0.2\ \text{Vs}^{-1}$.

[b] Average of the values derived from $E_p - E_{p/2}$ and $\partial E_p/\partial \log v$.

[c] $\Delta E_p = E_{p,M} - E_{p,GC}$, where $E_{p,M}$ and $E_{p,GC}$ are the peak potentials measured at M (Au or Ag) and GC, respectively.

Figure 1

DET mechanism	Leaving Group	
Stepwise with $\boxed{\kappa \rightarrow 1}$ ET kinetically more favoured, but thermodynamically less favoured	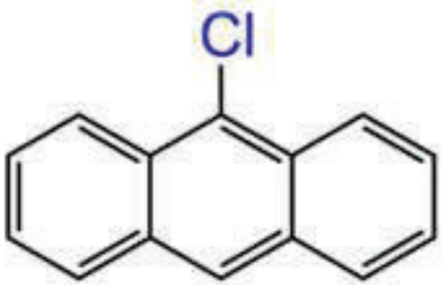 CA	 BA
Concerted $\boxed{\kappa = \alpha < 0.5}$ ET thermodynamically more favoured, but kinetically less favoured	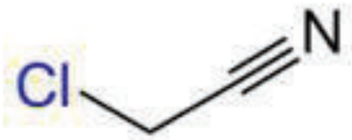 CAN	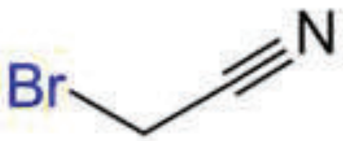 BAN

Figure 2

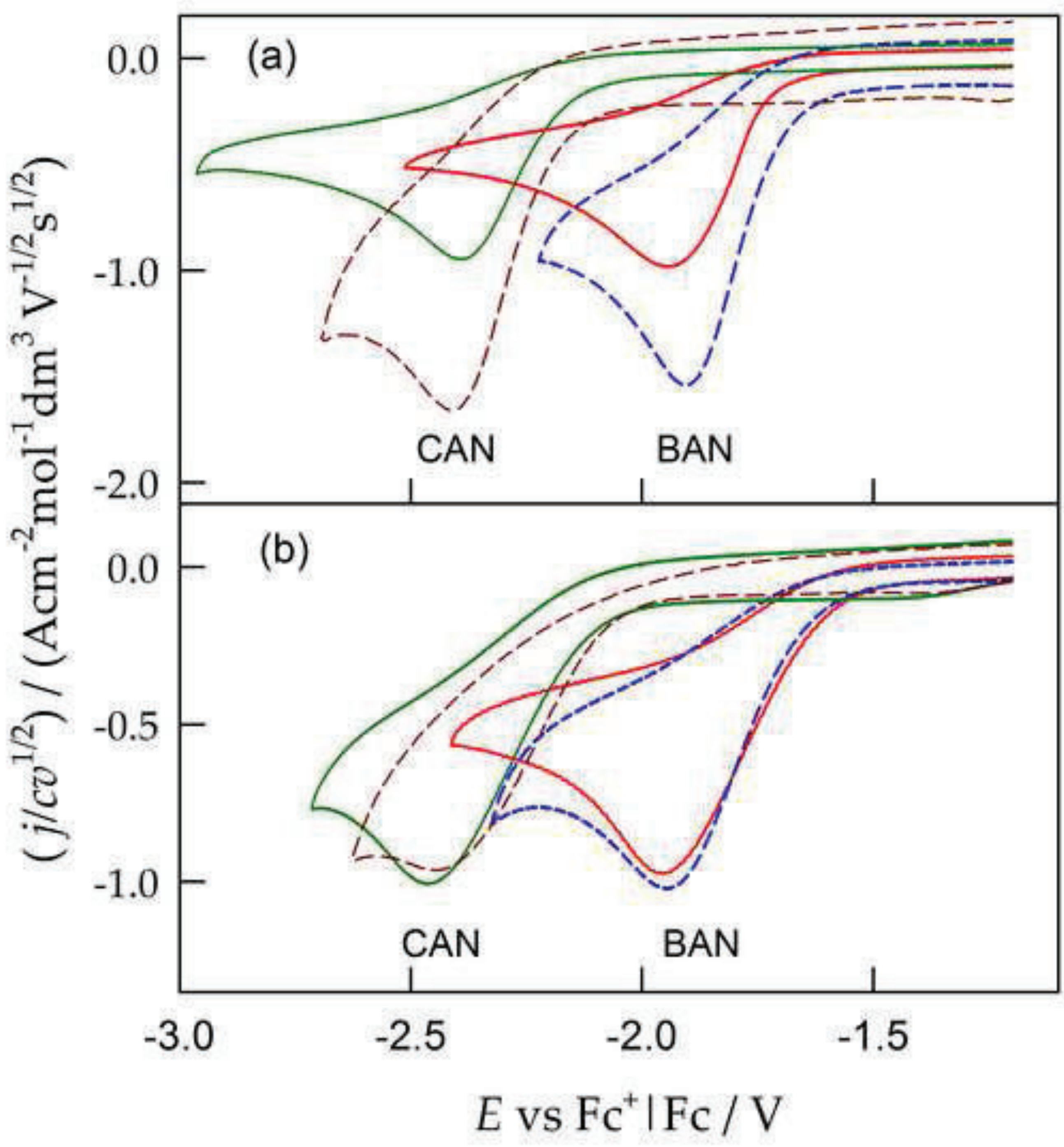
(a)
(b)
CAN
BAN
CAN
BAN
0.0
-1.0
-2.0
0.0
-0.5
-1.0
-3.0
-2.5
-2.0
-1.5
$(j/cv^{1/2})$ / (Acm^{-2}mol^{-1}dm^{3} V$^{-1/2}$s$^{1/2}$)
E vs Fc^{+}|Fc / V

Figure 3

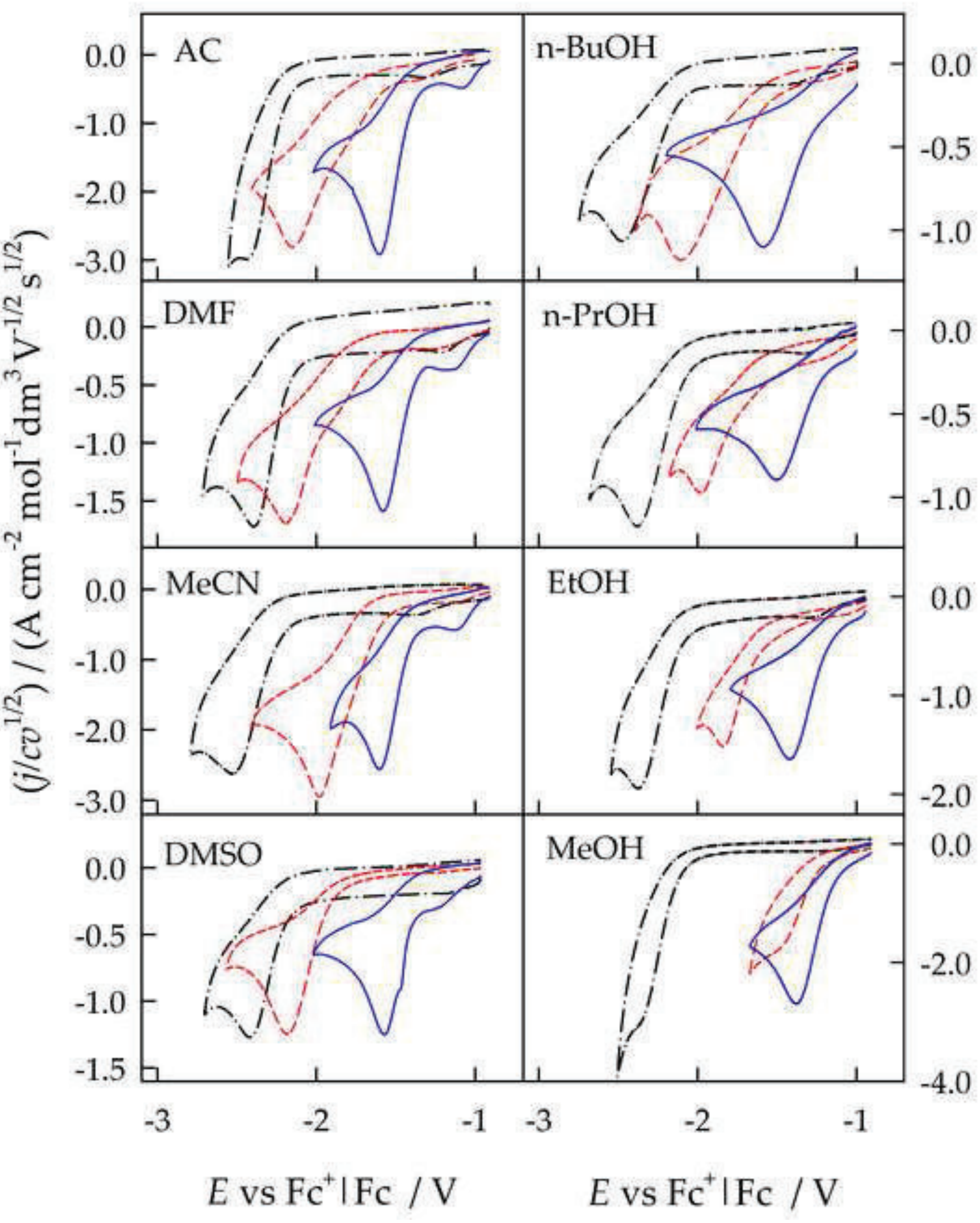
AC
n-BuOH
DMF
n-PrOH
MeCN
EtOH
DMSO
MeOH
0.0
-1.0
-2.0
-3.0
0.0
-0.5
-1.0
-1.5
0.0
-1.0
-2.0
-3.0
0.0
-0.5
-1.0
-1.5
0.0
-0.5
-1.0
0.0
-0.5
-1.0
0.0
-1.0
-2.0
0.0
-2.0
-4.0
(j/cv^1/2) / (A cm^-2 mol^-1 dm^3 V^-1/2 s^1/2)
-3
-2
-1
-3
-2
-1
E vs Fc+|Fc / V
E vs Fc+|Fc / V

Figure 4

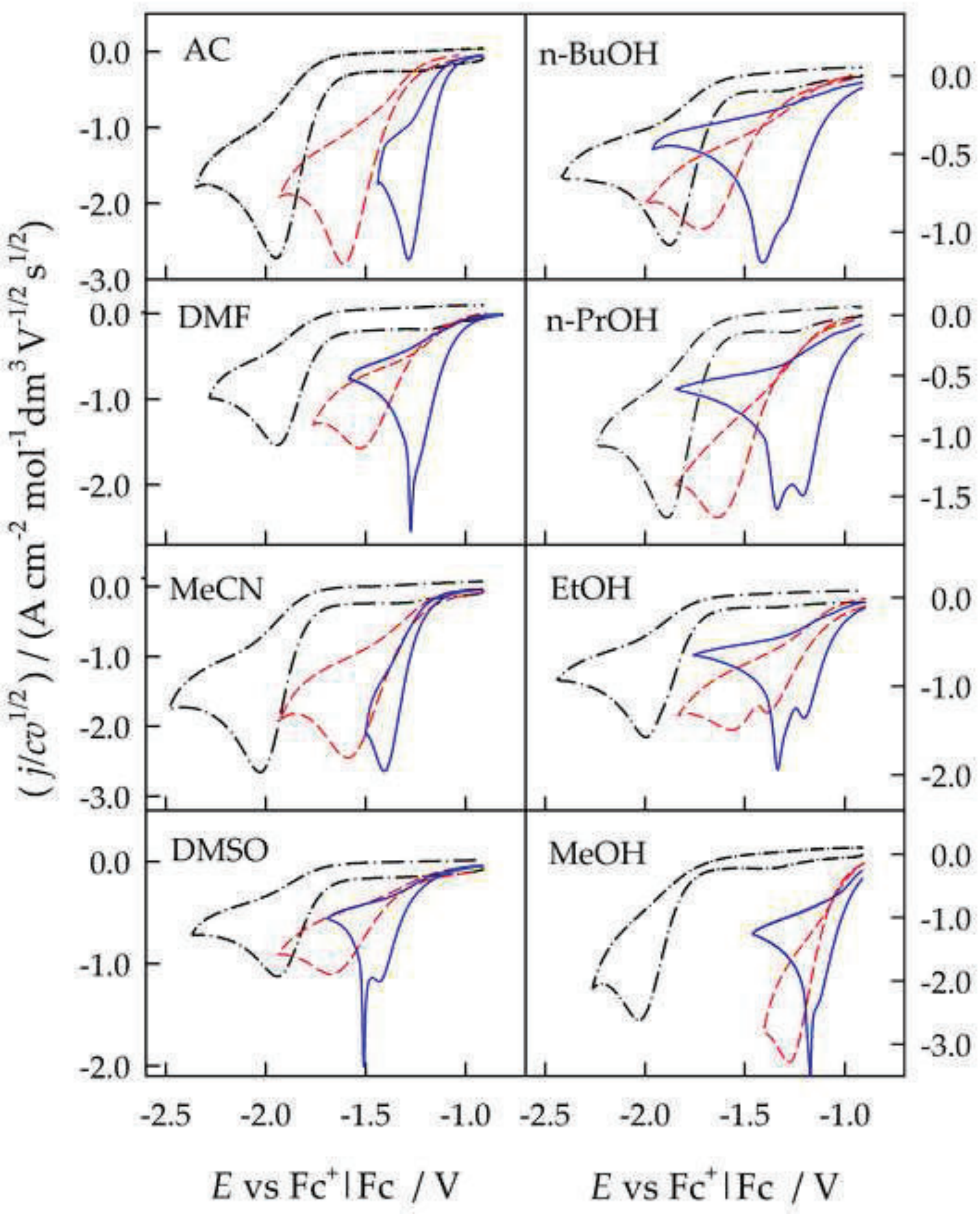
AC
n-BuOH
DMF
n-PrOH
MeCN
EtOH
DMSO
MeOH
(j/cv^1/2) / (A cm^-2 mol^-1 dm^3 V^-1/2 s^1/2)
0.0
-1.0
-2.0
-3.0
-0.5
-1.5
-2.5
-1.0
E vs Fc+|Fc / V

Figure 5

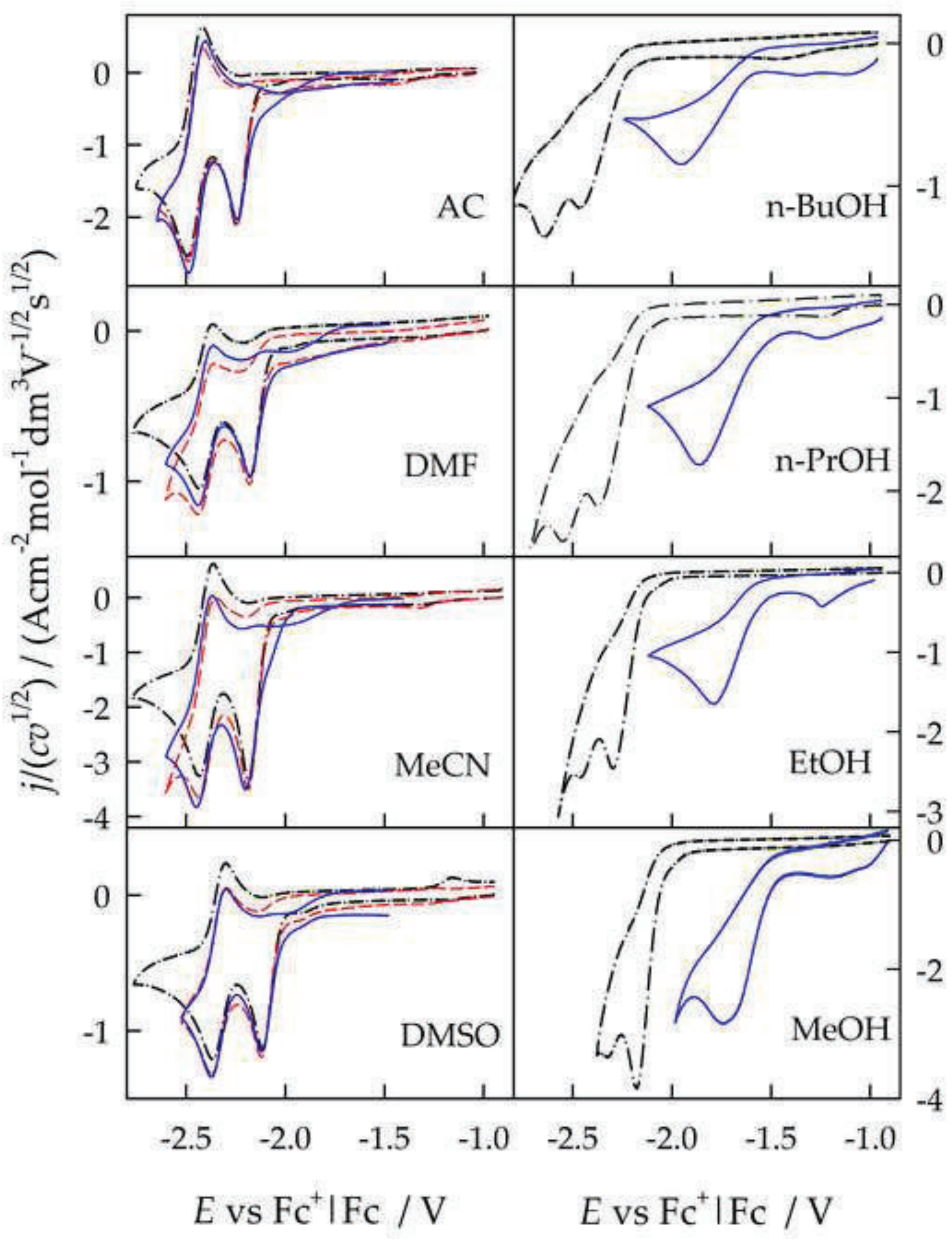
AC
DMF
MeCN
DMSO
n-BuOH
n-PrOH
EtOH
MeOH
$j/(cv^{1/2})$ / (Acm^{-2}mol^{-1}dm^{3}V$^{-1/2}$s$^{1/2}$)
0
-1
-2
-3
-4
-2.5
-2.0
-1.5
-1.0
E vs Fc^{+}|Fc / V
E vs Fc^{+}|Fc / V

Figure 6

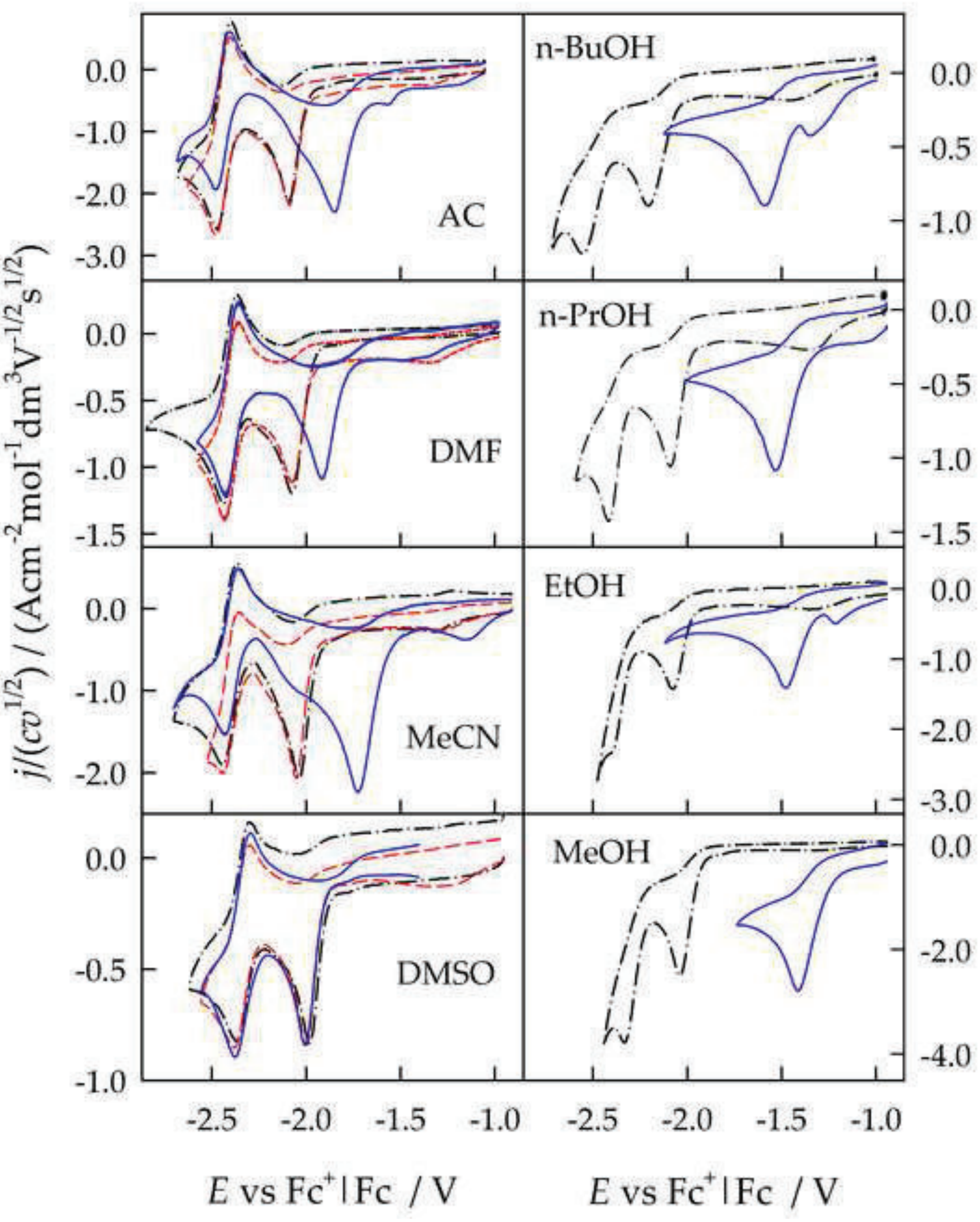
AC
DMF
MeCN
DMSO
n-BuOH
n-PrOH
EtOH
MeOH
0.0
-1.0
-2.0
-3.0
0.0
-0.5
-1.0
-1.5
0.0
-1.0
-2.0
0.0
-0.5
-1.0
0.0
-0.5
-1.0
0.0
-0.5
-1.0
-1.5
0.0
-1.0
-2.0
-3.0
0.0
-2.0
-4.0
-2.5
-2.0
-1.5
-1.0
-2.5
-2.0
-1.5
-1.0
$j/(cv^{1/2})$ / (Acm^{-2}mol^{-1}dm^{3}V$^{-1/2}$s$^{1/2}$)
E vs Fc$^+$|Fc / V
E vs Fc$^+$|Fc / V

Figure 7

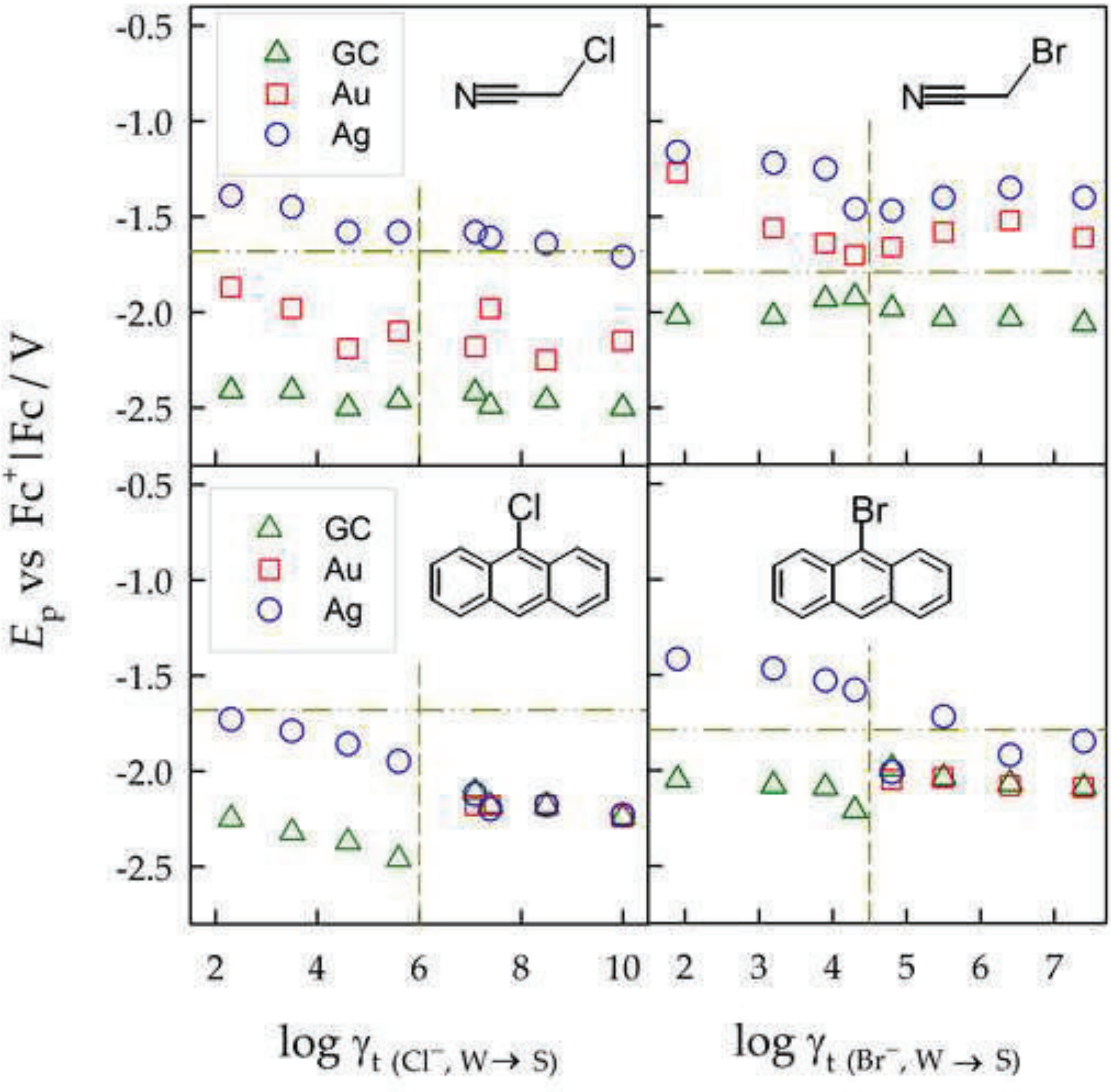
GC
Au
Ag
Cl
N
Br
-0.5
-1.0
-1.5
-2.0
-2.5
E_p vs Fc$^+$|Fc / V
2
4
6
8
10
3
5
7
log $\gamma_{t\,(Cl^-,\,W\rightarrow S)}$
log $\gamma_{t\,(Br^-,\,W\rightarrow S)}$

Figure 8

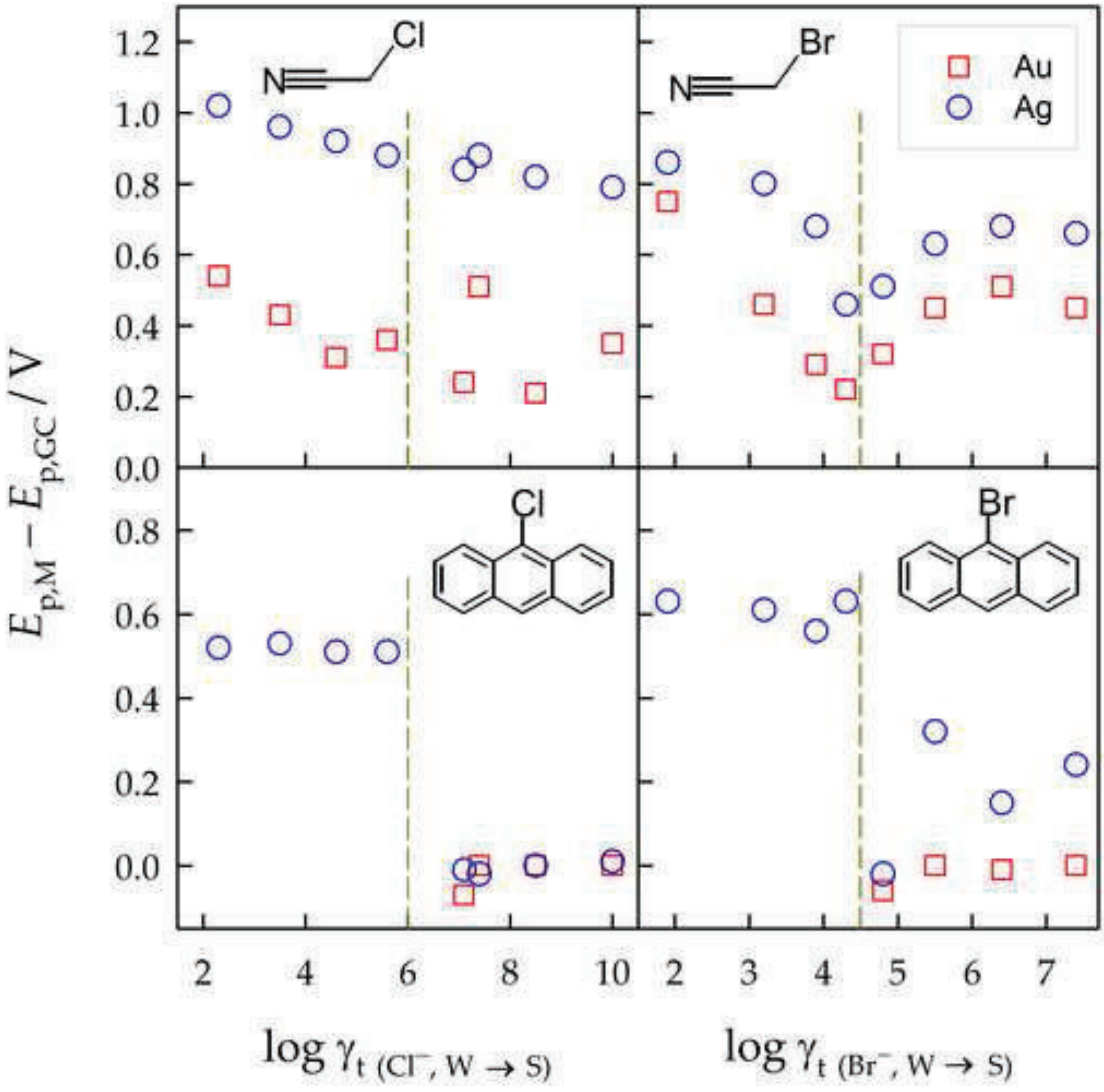
$E_{p,M} - E_{p,GC}$ / V
1.2
1.0
0.8
0.6
0.4
0.2
0.0
Cl
N
Br
Au
Ag
Cl
Br
2
4
6
8
10
2
3
4
5
6
7
$\log \gamma_{t\,(Cl^-,\,W \rightarrow S)}$
$\log \gamma_{t\,(Br^-,\,W \rightarrow S)}$

Figure 9

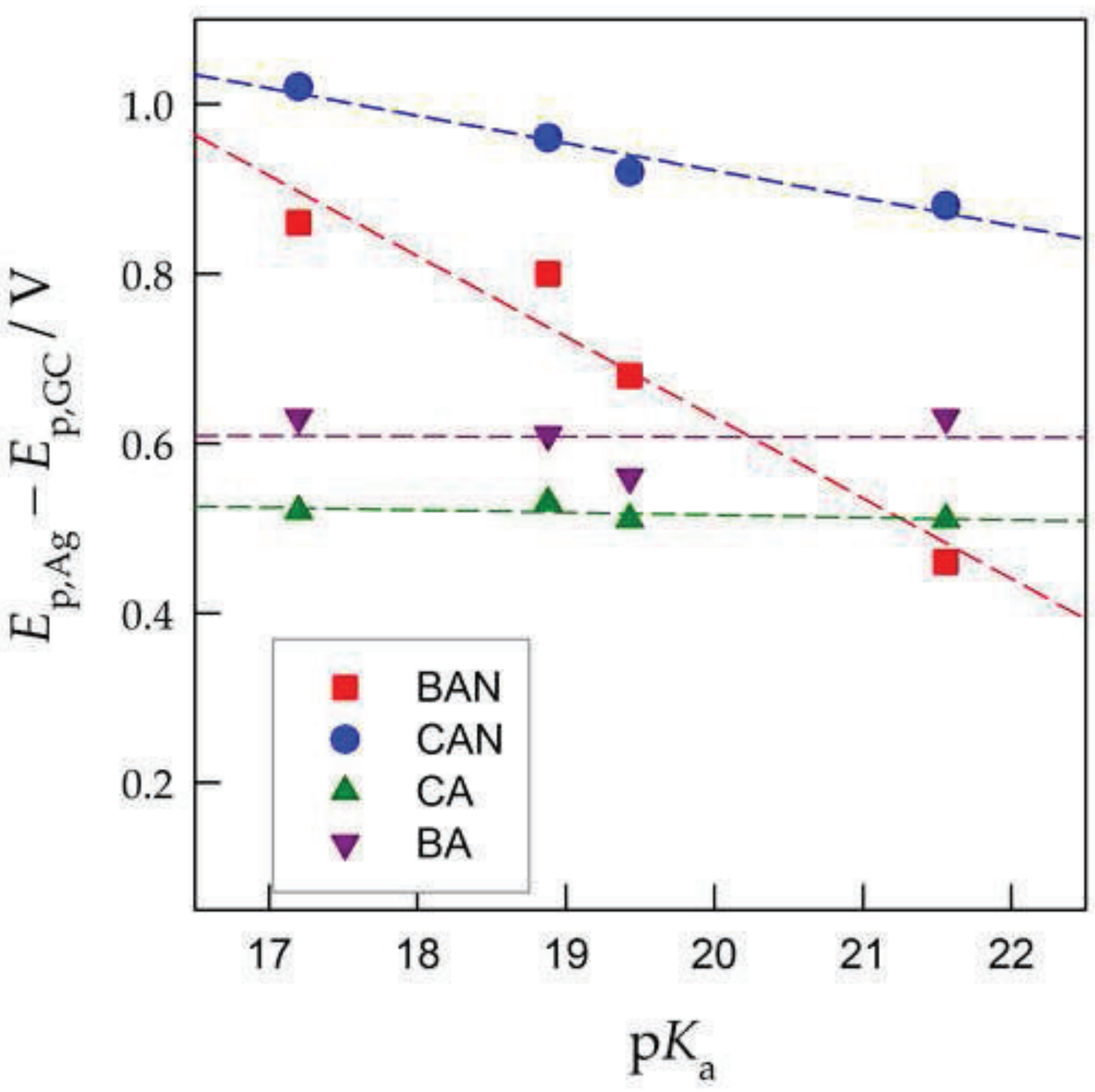

Scheme 1

(a)

$$\mathrm{ArX} + e^{-} \rightleftharpoons \mathrm{ArX}^{\bullet -}$$

$$\mathrm{ArX}^{\bullet -} \longrightarrow \mathrm{Ar}^{\bullet} + \mathrm{X}^{-}$$

$$\mathrm{Ar}^{\bullet} + e^{-} \rightleftharpoons \mathrm{Ar}^{-}$$

$$\mathrm{Ar}^{\bullet} + \mathrm{ArX}^{\bullet -} \rightleftharpoons \mathrm{Ar}^{-} + \mathrm{ArX}$$

$$\mathrm{Ar}^{-} + \mathrm{H}^{+} \longrightarrow \mathrm{ArH}$$

(b)

$$\mathrm{ArH} + e^{-} \rightleftharpoons \mathrm{ArH}^{\bullet -}$$

$$\mathrm{ArH}^{\bullet -} + \mathrm{H}^{+} \longrightarrow \mathrm{ArH}_2^{\bullet}$$

$$\mathrm{ArH}_2^{\bullet} + e^{-} \rightleftharpoons \mathrm{ArH}_2^{-}$$

$$\mathrm{ArH}_2^{\bullet} + \mathrm{ArH}^{\bullet -} \rightleftharpoons \mathrm{ArH}_2^{-} + \mathrm{ArH}$$

$$\mathrm{ArH}_2^{-} + \mathrm{H}^{+} \longrightarrow \mathrm{ArH}_3$$